

Manuscript version: Author's Accepted Manuscript

The version presented in WRAP is the author's accepted manuscript and may differ from the published version or Version of Record.

Persistent WRAP URL:

<http://wrap.warwick.ac.uk/143536>

How to cite:

Please refer to published version for the most recent bibliographic citation information. If a published version is known of, the repository item page linked to above, will contain details on accessing it.

Copyright and reuse:

The Warwick Research Archive Portal (WRAP) makes this work by researchers of the University of Warwick available open access under the following conditions.

© 2020 Elsevier. Licensed under the Creative Commons Attribution-NonCommercial-NoDerivatives 4.0 International <http://creativecommons.org/licenses/by-nc-nd/4.0/>.



Publisher's statement:

Please refer to the repository item page, publisher's statement section, for further information.

For more information, please contact the WRAP Team at: wrap@warwick.ac.uk.

An Approach to Predict Lower-order Dynamic Behaviors of a 5-DOF Hybrid Robot using a Minimum Set of Generalized Coordinates

Long Wu^a, Chenglin Dong^{a,*}, Guofeng Wang^a, Haitao Liu^a, Tian Huang^{a,b}

^a Key laboratory of Modern Mechanisms and Equipment Design of The State Ministry of Education, Tianjin University, Tianjin 300072, China

^b School of Engineering, The University of Warwick, Coventry CV4 7AL, UK

Abstract: This paper presents an effective semi-analytical approach for predicting lower-order dynamics of a five degrees-of-freedom (DOF) hybrid robot named TriMule, which is composed of a 3-DOF parallel mechanism plus a 2-DOF A/C wrist. In this method, the governing equations of motion of limbs within the parallel mechanism are first formulated by finite element analysis (FEA) and then reduced to super-element models. This is followed by exploiting a general stiffness model of multiple DOF joints connecting the super-elements. These two threads lead to the reduced dynamic model of the parallel mechanism while keeping the full set of lower-order modes retained. Finally, the dynamic model of entire system is established by merging the models of parallel mechanism and wrist. The computational results show that the lower-order natural frequencies, mode shapes of the entire system, and the frequency response functions (FRFs) of the robot tool center point (TCP) estimated by the proposed approach have very good agreement with those obtained by a full order FE model and experimental modal tests. The merits of this approach lie in that the established model allows the full set of lower-order dynamics of the entire system to be predicted effectively and accurately by only using fourteen generalized coordinates.

Keywords: Parallel kinematic machines; Substructure synthesis; Dynamics of multi-body systems

1. Introduction

Dynamic behavior is one of the most important performance factors of parallel kinematic machines (PKMs) especially for those developed for machining purposes, drilling and/or milling for example, where the end-effector is excited by dynamic loadings caused by tool-workpiece interaction. Since dynamics of PKMs is highly pose-dependent, it essentially requires a model that enables the full set of lower-order dynamics to be predicted efficiently and accurately, an important issue for dimensional/structural optimization as well as for cutting stability analysis [1-3] under the framework of digitalized design.

In the last few decades, intensive studies have been carried out for dynamic modeling of PKMs. The methods available at hand can roughly be classified into three categories, i.e. full order Finite Element Analysis (FEA) [4-7], lumped parameter methods [8-11] and semi-analytical methods [12-27]. Combining fundamental robotics with structural dynamics, it has been well recognized that the semi-analytical approach is particularly useful for the predesign stage thanks to its much lower computational cost compared to full order FE models. Along this track, several approaches have been proposed, known as Matrix Structure Analysis (MSA) [12-16], Virtual Joint Method (VJM) [17-20] and Component Mode Synthesis (CMS) [21-24]. In the MSA method, the flexible links are frequently treated as spatial beam elements. In the VJM method, the flexible links are simplified as a number of discrete lumped mass-springs using the finite segment concept [28]. In the CMS method, the degrees-of-freedom (DOFs) of a flexible link modeled by a full order FE model are significantly reduced using substructure synthesis technique while keeping the lower-order modes almost unchanged. This approach has been successfully applied to dynamic modelling and cutting stability analysis of a PKM based machine tool [22], demonstrating a great potential for the improvement of computational efficiency compared with FEA.

More recently, several interesting attempts have been made toward achieving ‘simpler’ dynamic models having smaller number of DOFs. For example, Briot *et al.* [25] proposed a general and systematic approach for predicting the first six modes of parallel mechanisms. In this method, the Rayleigh-Ritz approximation was employed to form the bases that link the deflection twist of the end-effector with a set of generalized coordinates. Zhang *et al.* [26] proposed an approximate approach for dynamic modeling of a 3-PRS parallel mechanism designed for high speed machining. In this method, the Cartesian mass matrix was derived by assuming all links as rigid bodies, while the Cartesian stiffness matrix was modeled by considering compliances along/about the screw axes of static wrenches imposed by the limbs upon the platform. The authors claimed that the proposed model enables the first and second order natural frequencies to be predicted with sufficient accuracy. Drawing mainly upon work-energy method, Dong *et al.* [27] presented an approach for dynamic modeling of the well-known Tricept robot developed for both milling and optical polishing. In this method, static condensation technique was employed that leads to a 9-DOF dynamic model containing the 6-dimensional

* Corresponding author.

E-mail addresses: chenglindong_tju@tju.edu.cn (C. Dong)

deflections of the end-effector and three rotational deflections about the axes of a 3-DOF wrist. Although axial compliances of three actuated limbs were fully considered, their idle motions were treated as rigid body motions. This over-simplified treatment, however, cause the ignorance of lower-order bending modes that would have significant bearings on the FRFs at the robot TCP.

Combining screw theory with modal reduction technique, this paper deals with dynamic modeling of a 5-DOF hybrid robot named TriMule. Its particular goal is twofold: (1) to develop an approach that enables the full set of lower-order modes affecting frequency response functions of the robot TCP to be predicted accurately and effectively using a minimum set of generalized coordinates that include those reflecting the first-order elastic bending modes; (2) to develop a general method for stiffness modelling of passive joints, an important issue in dynamic modelling of parallel mechanisms. After this brief review to the dynamic modelling of PKMs in Section 1, the description of the TriMule robot is introduced in Section 2. Section 3 starts with the formulation of the reduced dynamic model of the parallel mechanism by developing the super-element models of all substructures and the general stiffness model of multiple DOF joints connecting the super-elements. Then, it follows dynamic modelling of the entire system via merging the elastic potential and kinetic energies of the parallel mechanism and wrist. In Section 4, a full-size TriMule robot is taken as an exemplar for illustrating the effectiveness of the proposed approach by calculating the lower-order dynamic behaviors and comparing them with those obtained by a full order FE model. The conclusions are drawn in Section 5.

2. System Description

Fig.1 shows a 3D view of the TriMule robot under consideration, which essentially consists of a 1T2R (T-Translation, R-Rotation) spatial parallel mechanism for positioning and an A/C wrist attached to the platform for orientating. The 1T2R parallel mechanism consists of a 6-DOF UPS limb plus a 2-DOF planar parallel mechanism comprising two actuated RPS limbs and a passive RP limb in the middle. The base link of the planar parallel mechanism is connected with the machine frame by a pair of R joints. Here, R, P, U, and S denote revolute, prismatic, universal and spherical joints, and the underlined P denotes an actuated prismatic joint. Note that the S and U joints are formed by the appropriate number of R joints having mutually orthogonal axes. For convenience, we number three actuated limbs as limbs 1, 2 and 3, and the passive limb as limb 4. For the detailed description of the robot, please refer to [29, 30].

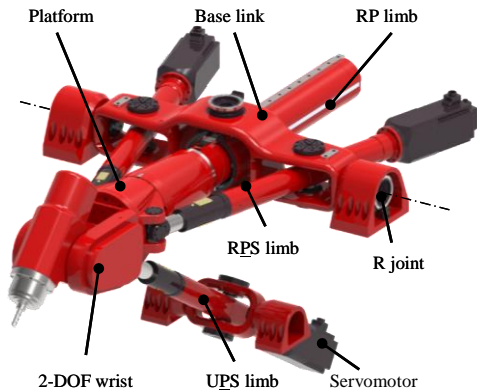


Fig.1. 3D view of the TriMule robot

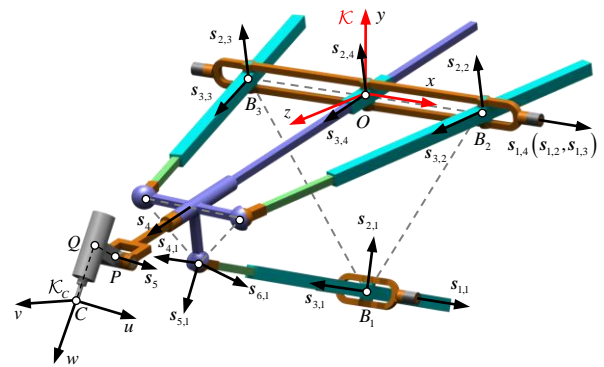


Fig.2. Schematic diagram of the TriMule robot

Fig.2 shows the schematic diagram of the hybrid robot, where some special points at machine frame, platform, wrist and end-effector are represented by O , P , Q and C . The reference frame, denoted by \mathcal{K} , is placed at O with its x axis coincident with the axis of the R joint connecting the base link with the machine frame, and its z axis normal to the equilateral triangle $\Delta B_1 B_2 B_3$. A body fixed frame, denoted by \mathcal{K}_c , is attached to the end-effector at C , a milling spindle for example, with its w axis coincident with the tool axis, and its u axis parallel to the A-axis of the wrist. The unit vectors of joint axes shown in Fig.2 satisfy the relationships below

$$\begin{aligned} \mathbf{s}_{1,1} &= \mathbf{s}_{1,2} = \mathbf{s}_{1,3} = \mathbf{s}_{1,4} \\ \mathbf{s}_{1,i} &\perp \mathbf{s}_{2,i}, \mathbf{s}_{2,i} \perp \mathbf{s}_{3,i}, \mathbf{s}_{3,i} = \mathbf{s}_{4,i}, \mathbf{s}_{4,i} \perp \mathbf{s}_{5,i}, \mathbf{s}_{5,i} \perp \mathbf{s}_{6,i}, \quad i=1,2,3 \\ \mathbf{s}_{1,4} &\perp \mathbf{s}_{2,4}, \mathbf{s}_{2,4} \perp \mathbf{s}_{3,4}, \mathbf{s}_{3,4} = \mathbf{s}_4, \mathbf{s}_4 \perp \mathbf{s}_5 \end{aligned} \quad (1)$$

Hereafter, we assume that all vectors and matrices are expressed in \mathcal{K} unless indicated otherwise.

3. Dynamic Modeling of the Hybrid Robot

For dynamic modeling, we lock all actuated joints such that the entire system can be visualized as an instantaneous structure at a given configuration. Then, we formulate dynamic models of the parallel mechanism and the hybrid robot as a whole sequentially and concentrate on developing an effective method that enables the lower-order dynamics of the end-effector to be retained using a minimum set of generalized coordinates.

3.1 Modeling of the parallel mechanism

3.1.1 Super-element modeling of substructures

The first step in dynamic modeling of parallel mechanism is to decompose it into five substructures and then build their super-element models by FEA and modal reduction technique. In order to do so, the base link and the four limb-bodies are sequentially numbered from 0 to 4, as depicted in Fig.3. For convenience, set a number of nodes, denoted by 'N' with the appropriate local subscripts at key points of a substructure. Among them the nodes denoted also by 'A' are the interface (or external) nodes that link the substructure with others or with the machine frame via single or multiple DOF joints.

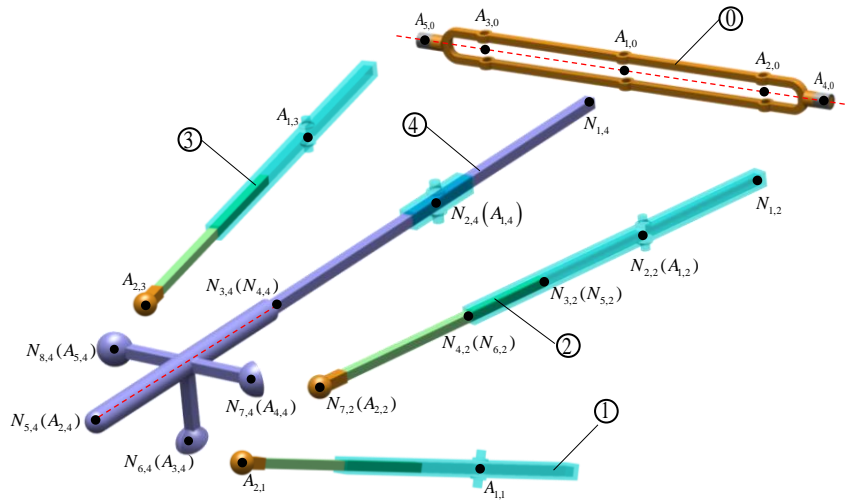


Fig.3. Substructures within the parallel mechanism

With this convention, we first formulate the super-element model of the i th ($i=1,2,3$) telescopic actuated limb-body as detailed in Fig.4, which comprises a thrust rod and a sleeve connected via an internal \underline{P} joint driven by a screw-nut-motor assembly. In the modelling, the sleeve is treated as a spatial elastic beam having four nodes $N_{1,i} \sim N_{4,i}$, the thrust rod as that having three nodes $N_{5,i} \sim N_{7,i}$, and the servo motor as a lumped mass situated at $N_{1,i}$. Note that $N_{2,i}$ is connected internally with $N_{5,i}$ by a linear spring to model axial compliance of the screw-nut assembly. Also, note that there exists a relative axial deflection between $N_{3,i}$ ($N_{4,i}$) and $N_{5,i}$ ($N_{6,i}$) while remaining their deflections in other directions identical. Two interface nodes $A_{j,i}$ ($j=1,2$) are assigned such that they connect the limb-body with the machine frame or the base link by a U or R joint at $A_{1,i}$, and with the platform by an S joint at $A_{2,i}$.

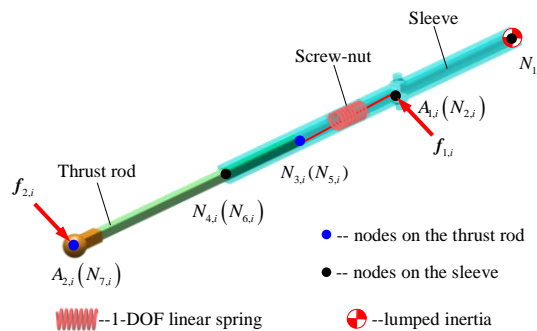


Fig.4. Finite element model of the actuated limb-body

Modeling the two spatial elastic beams by FEA and assembling them using the geometric and physical boundary conditions mentioned above, leads to the dynamic model of the limb-body

$$\begin{bmatrix} \mathbf{M}_{xx,i} & \mathbf{M}_{x\eta,i} \\ \mathbf{M}_{x\eta,i}^T & \mathbf{M}_{\eta\eta,i} \end{bmatrix} \begin{pmatrix} \ddot{\mathbf{x}}_i \\ \ddot{\boldsymbol{\eta}}_i \end{pmatrix} + \begin{bmatrix} \mathbf{K}_{xx,i} & \mathbf{K}_{x\eta,i} \\ \mathbf{K}_{x\eta,i}^T & \mathbf{K}_{\eta\eta,i} \end{bmatrix} \begin{pmatrix} \mathbf{x}_i \\ \boldsymbol{\eta}_i \end{pmatrix} = \begin{pmatrix} \mathbf{f}_i \\ \mathbf{0} \end{pmatrix}, \quad i = 1, 2, 3 \quad (2)$$

$$\mathbf{x}_i = \begin{pmatrix} \xi_{1,i} \\ \xi_{2,i} \end{pmatrix}, \quad \mathbf{f}_i = \begin{pmatrix} f_{1,i} \\ f_{2,i} \end{pmatrix}$$

where $\mathbf{M}_{xx,i}$, $\mathbf{M}_{x\eta,i}$ and $\mathbf{M}_{\eta\eta,i}$ ($\mathbf{K}_{xx,i}$, $\mathbf{K}_{x\eta,i}$ and $\mathbf{K}_{\eta\eta,i}$) represent the partitioned mass (stiffness) matrices associated with the generalized coordinates $(\mathbf{x}_i^T \ \boldsymbol{\eta}_i^T)^T$; $\mathbf{f}_{j,i} \in \mathbb{R}^6$ and $\boldsymbol{\xi}_{j,i} \in \mathbb{R}^6$ ($j=1,2, i=1,2,3$) are the nodal force and deflection vectors at $A_{j,i}$; $\boldsymbol{\eta}_i$ is the collection of the nodal deflections of all the internal nodes.

According to the modal reduction method [31-33], let $(\mathbf{x}_i^T \ \boldsymbol{\eta}_i^T)^T$ be expressed as

$$\begin{pmatrix} \mathbf{x}_i \\ \boldsymbol{\eta}_i \end{pmatrix} = \begin{bmatrix} \mathbf{1}_{12} & \mathbf{0} \\ \mathbf{B}_i & \boldsymbol{\Phi}_i \end{bmatrix} \begin{pmatrix} \mathbf{x}_i \\ \mathbf{p}_i \end{pmatrix}, \quad i = 1, 2, 3 \quad (3)$$

$$\mathbf{B}_i = -\mathbf{K}_{\eta\eta,i}^{-1} \mathbf{K}_{x\eta,i}^T, \quad \boldsymbol{\Phi}_i = [\boldsymbol{\phi}_{1,i} \ \boldsymbol{\phi}_{2,i} \ \boldsymbol{\phi}_{3,i}], \quad \mathbf{p}_i = (p_{1,i} \ p_{2,i} \ p_{3,i})^T$$

where $\boldsymbol{\phi}_{1,i}$ and $\boldsymbol{\phi}_{2,i}$ are the first-order internal bending modes about two orthogonal axes normal to the axial axis of the limb-body, $\boldsymbol{\phi}_{3,i}$ is the first-order internal extension/compression mode along the axial axis. These internal modes can be determined by solving the eigenvalue problem $[\mathbf{K}_{\eta\eta,i} - \lambda \mathbf{M}_{\eta\eta,i}] \boldsymbol{\phi} = \mathbf{0}$ provided that $\boldsymbol{\xi}_{j,i} = \mathbf{0}$ ($j=1,2$); $p_{k,i}$ is the internal modal coordinate associated with $\boldsymbol{\phi}_{k,i}$ ($k=1,2,3$).

Consequently, substituting Eq. (3) into Eq. (2), and left-multiplying the transpose of the relevant coordinate transformation matrix given in Eq. (3), results in the super-element model of the limb-body

$$\mathbf{M}_i \begin{pmatrix} \ddot{\mathbf{x}}_i \\ \ddot{\mathbf{p}}_i \end{pmatrix} + \mathbf{K}_i \begin{pmatrix} \mathbf{x}_i \\ \mathbf{p}_i \end{pmatrix} = \begin{pmatrix} \mathbf{f}_i \\ \mathbf{0} \end{pmatrix}, \quad i = 1, 2, 3 \quad (4)$$

$$\mathbf{M}_i = \begin{bmatrix} \mathbf{1}_{12} & \mathbf{0} \\ \mathbf{B}_i & \boldsymbol{\Phi}_i \end{bmatrix}^T \begin{bmatrix} \mathbf{M}_{xx,i} & \mathbf{M}_{x\eta,i} \\ \text{sym} & \mathbf{M}_{\eta\eta,i} \end{bmatrix} \begin{bmatrix} \mathbf{1}_{12} & \mathbf{0} \\ \mathbf{B}_i & \boldsymbol{\Phi}_i \end{bmatrix}, \quad \mathbf{K}_i = \begin{bmatrix} \mathbf{1}_{12} & \mathbf{0} \\ \mathbf{B}_i & \boldsymbol{\Phi}_i \end{bmatrix}^T \begin{bmatrix} \mathbf{K}_{xx,i} & \mathbf{K}_{x\eta,i} \\ \text{sym} & \mathbf{K}_{\eta\eta,i} \end{bmatrix} \begin{bmatrix} \mathbf{1}_{12} & \mathbf{0} \\ \mathbf{B}_i & \boldsymbol{\Phi}_i \end{bmatrix}$$

Then, we consider dynamic modelling of the passive limb-body that comprises a central tube and a platform rigidly connected to the tube as indicated in Fig.5. The central tube is treated as a spatial elastic beam having three nodes $N_{1,4} \sim N_{3,4}$, and the platform as a rigid body having five nodes $N_{4,4} \sim N_{8,4}$. Five interface nodes $A_{j,4}$ ($j=1 \sim 5$) are set for the limb-body to connect with the base link by a compound RP joint at $A_{1,4}$, with the wrist by an actuated $\underline{\mathbf{R}}$ joint at $A_{2,4}$, and with three actuated limbs by S joints at $A_{3,4}$, $A_{4,4}$ and $A_{5,4}$, respectively.

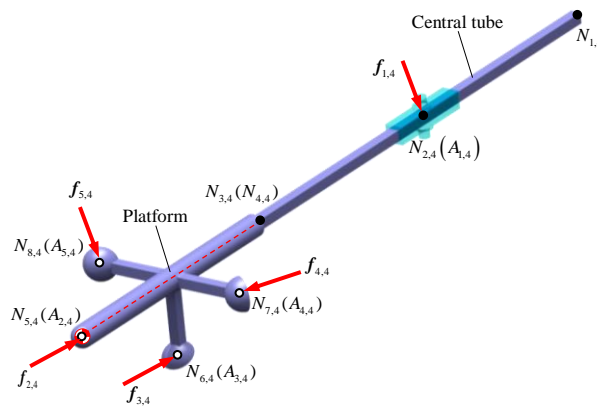


Fig.5. Finite element model of the passive limb-body

Using the identical method for formulating Eq. (4), yields the super-element model of the limb-body

$$\mathbf{M}_4 \begin{pmatrix} \ddot{\mathbf{x}}_4 \\ \ddot{\mathbf{p}}_4 \end{pmatrix} + \mathbf{K}_4 \begin{pmatrix} \mathbf{x}_4 \\ \mathbf{p}_4 \end{pmatrix} = \begin{pmatrix} \mathbf{f}_4 \\ \mathbf{0} \end{pmatrix} \quad (5)$$

$$\mathbf{x}_4 = \begin{pmatrix} \xi_{1,4} \\ \xi_{2,4} \end{pmatrix}, \quad \mathbf{p}_4 = \begin{pmatrix} p_{1,4} \\ p_{2,4} \\ p_{3,4} \end{pmatrix}, \quad \mathbf{f}_4 = \begin{pmatrix} \mathbf{f}_{1,4} \\ \sum_{j=2}^5 \mathbf{T}_{j,4}^{-T} \mathbf{f}_{j,4} \end{pmatrix}, \quad \xi_{j,4} = \mathbf{T}_{j,4} \xi_{2,4}, \quad \mathbf{T}_{j,4} = \begin{bmatrix} \mathbf{1}_3 & [\mathbf{r}_{j,4} \times] \\ \mathbf{0} & \mathbf{1}_3 \end{bmatrix}, \quad j = 2 \sim 5$$

where \mathbf{M}_4 and \mathbf{K}_4 represent the mass and stiffness matrices associated with the generalized coordinates $(\mathbf{x}_4^T \quad \mathbf{p}_4^T)^T$; $\mathbf{f}_{j,4} \in \mathbb{R}^6$ and $\xi_{j,4} \in \mathbb{R}^6$ ($j=1 \sim 5$) are the interface nodal force and deflection vectors at $A_{j,4}$; $p_{1,4}$, $p_{2,4}$ and $p_{3,4}$ are the internal modal coordinates associated with the first-order torsional and bending modes of the limb-body, respectively; $[\mathbf{r}_{j,4} \times]$ is the skew-symmetric matrix of $\mathbf{r}_{j,4} = \overline{A_{2,4}A_{j,4}}$.

Finally, with the convention of symbolic notations used in Eq. (5), the dynamic model of the base link shown in Fig.6 can be formulated with ease by treating it as a rigid body because of its much higher rigidity compared with other substructures involved

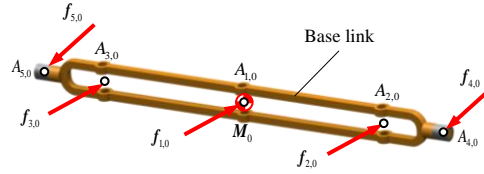


Fig.6. Rigid body model of the base link

$$\mathbf{M}_0 \ddot{\xi}_{1,0} = \sum_{j=1}^5 \mathbf{T}_{j,0}^{-T} \mathbf{f}_{j,0} \quad (6)$$

$$\xi_{j,0} = \mathbf{T}_{j,0} \xi_{1,0}, \quad \mathbf{T}_{j,0} = \begin{bmatrix} \mathbf{1}_3 & [\mathbf{r}_{j,0} \times] \\ \mathbf{0} & \mathbf{1}_3 \end{bmatrix}, \quad j = 1 \sim 5$$

where $\mathbf{M}_0 \in \mathbb{R}^{6 \times 6}$ is the mass matrix of the base link evaluated at $A_{1,0}$; $\mathbf{f}_{j,0} \in \mathbb{R}^6$ and $\xi_{j,0} \in \mathbb{R}^6$ ($j=1 \sim 5$) are the nodal force and deflection vectors at $A_{j,0}$; $\mathbf{r}_{j,0} = \overline{A_{1,0}A_{j,0}}$.

3.1.2 Stiffness modeling of multiple-DOF passive joints

This section presents a general method for stiffness modeling of multiple-DOF passive joints commonly used in the spatial mechanism having closed loops. This model therefore is applicable to the joint stiffness modeling of the parallel mechanism under consideration. Without loss of generality, let $A_{u,i}$ and $A_{v,j}$ be two interface nodes belonging to substructures S_i and S_j , and be connected by the n th ($n=1,2,\dots,N$) passive joint having M_n DOF, as depicted in Fig.7. Since $A_{u,i}$ and $A_{v,j}$ are coincident at the equilibrium pose, let A_n be the point having the same coordinates. Place a reference frame \mathcal{K}_n at A_n with its three orthogonal axes being parallel to those of \mathcal{K} .

A method is now developed to derive the general expression of stiffness matrix of the n th passive joint in terms of stiffness matrices of M_n serially connected elastic elements whose compliances are defined in a set of local body-fixed frames $\mathcal{K}_{m,n}$ ($m=1,2,\dots,M_n$). Each elastic element represents compliances of either a 1-DOF revolute or prismatic joint with the joint axis coincident with the $z_{m,n}$ axis of $\mathcal{K}_{m,n}$. Evaluated in $\mathcal{K}_{m,n}$, let $\alpha_{m,n} \in \mathbb{R}^5$, $\beta_{m,n} \in \mathbb{R}^5$ and $\mathbf{K}_{m,n} \in \mathbb{R}^{5 \times 5}$ be the reaction vector, deflection vector and stiffness matrix of the m th element in the n th passive joint. Then, the Hooks' law gives

$$\alpha_{m,n} = \mathbf{K}_{m,n} \beta_{m,n} \quad (7)$$

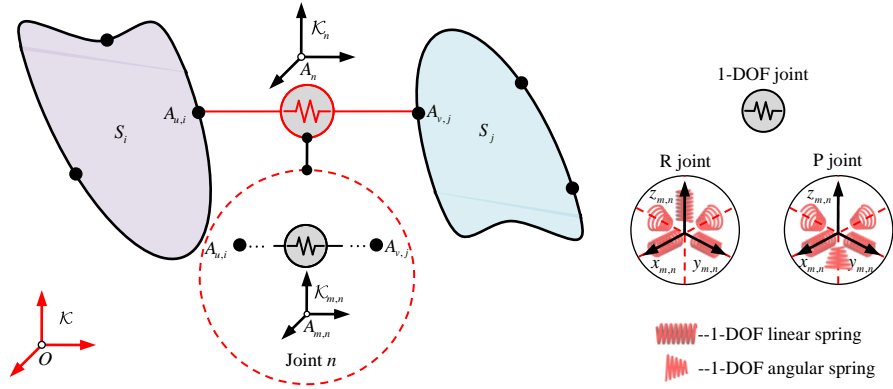


Fig.7. M_n -DOF passive joint at A_n

On one hand, in the light of screw theory and Newton's third law, the nodal force vector $\mathbf{f}_n = \mathbf{f}_{u,i} = -\mathbf{f}_{v,j} \in \mathbb{R}^6$ between two substructures at A_n ($A_{u,i}$, $A_{v,j}$) can be expressed as a linear combination of $6 - M_n$ independent unit constraint wrenches, i.e.

$$\mathbf{f}_n = \sum_{l=1}^{6-M_n} \bar{\alpha}_{l,n} \hat{\mathbf{f}}_{l,n} = \mathbf{W}_n \bar{\alpha}_n \quad (8)$$

$$\mathbf{W}_n = [\hat{\mathbf{f}}_{1,n} \quad \cdots \quad \hat{\mathbf{f}}_{6-M_n,n}], \quad \bar{\alpha}_n = (\bar{\alpha}_{1,n} \quad \cdots \quad \bar{\alpha}_{6-M_n,n})^T$$

where $\hat{\mathbf{f}}_{l,n} \in \mathbb{R}^6$ is the l th ($l=1,2,\dots,6-M_n$) unit constraint wrench and $\bar{\alpha}_{l,n}$ is its intensity.

On the other hand, let $\boldsymbol{\zeta}_n \in \mathbb{R}^6 = \boldsymbol{\zeta}_{u,i} - \boldsymbol{\zeta}_{v,j}$ be the relative deflection vector between $A_{u,i}$ and $A_{v,j}$, where $\boldsymbol{\zeta}_{u,i} \in \mathbb{R}^6$ and $\boldsymbol{\zeta}_{v,j} \in \mathbb{R}^6$ be the nodal deflection vectors at $A_{u,i}$ and $A_{v,j}$, respectively. For the M_n -DOF passive joint at A_n , $\boldsymbol{\zeta}_n$ can be decomposed into

$$\boldsymbol{\zeta}_n = \boldsymbol{\zeta}_n^e + \boldsymbol{\zeta}_n^r \quad (9)$$

where $\boldsymbol{\zeta}_n^e \in \mathbb{R}^6$ represents elastic deflections while $\boldsymbol{\zeta}_n^r$ arises from the combined rigid body motions necessary to satisfy geometric compatibility conditions among the substructures when the actuated joints are locked. Note that $\hat{\mathbf{f}}_{l,n}$ and therefore \mathbf{f}_n only delivers work on $\boldsymbol{\zeta}_n^e$, so, left-multiplying both sides of Eq. (9) with \mathbf{W}_n^T , leads to

$$\mathbf{W}_n^T \boldsymbol{\zeta}_n = \mathbf{W}_n^T \boldsymbol{\zeta}_n^e = \bar{\boldsymbol{\beta}}_n, \quad \mathbf{W}_n^T \boldsymbol{\zeta}_n^r = \mathbf{0} \quad (10)$$

where $\bar{\boldsymbol{\beta}}_n = (\bar{\beta}_{1,n} \quad \cdots \quad \bar{\beta}_{6-M_n,n})^T$ with $\bar{\beta}_{l,n}$ ($l=1,2,\dots,6-M_n$) being the corresponding deflection caused by $\bar{\alpha}_{l,n}$.

Because all the elastic elements are connected serially, $\boldsymbol{\zeta}_n^e$ can be written as the sum of $\boldsymbol{\zeta}_{m,n}^e$ ($m=1,\dots,M_n$) under the action of \mathbf{f}_n

$$\boldsymbol{\zeta}_n^e = \sum_{m=1}^{M_n} \boldsymbol{\zeta}_{m,n}^e \quad (11)$$

where $\boldsymbol{\zeta}_{m,n}^e \in \mathbb{R}^6$ represents the elastic deflection twist caused by the m th elastic element.

Hence, the principle of virtual work gives

$$\boldsymbol{\zeta}_{m,n}^e = \mathbf{T}_{m,n} \boldsymbol{\beta}_{m,n}, \quad \boldsymbol{\alpha}_{m,n} = \mathbf{T}_{m,n}^T \mathbf{f}_n \quad (12)$$

where $\mathbf{T}_{m,n}$ is the matrix that transforms $\boldsymbol{\beta}_{m,n}$ defined in $\mathcal{K}_{m,n}$ to $\boldsymbol{\zeta}_{m,n}^e$ defined in \mathcal{K}_n , and it can be obtained by removing an appropriate column of the adjoint transform matrix $\mathbf{T}'_{m,n}$ of $\mathcal{K}_{m,n}$ with respect to \mathcal{K}_n . For a prismatic

joint, the third column of $\mathbf{T}'_{m,n}$ should be removed, otherwise the sixth column of $\mathbf{T}'_{m,n}$ should be removed for an revolute joint. $\mathbf{T}'_{m,n}$ is of the form below

$$\mathbf{T}'_{m,n} = \begin{bmatrix} \mathbf{R}_{m,n} & [\mathbf{r}_{m,n} \times] \mathbf{R}_{m,n} \\ \mathbf{0} & \mathbf{R}_{m,n} \end{bmatrix} \in \mathbb{R}^{6 \times 6} \quad (13)$$

where $\mathbf{R}_{m,n} \in \mathbb{R}^{3 \times 3}$ represents the orientation matrix of $\mathcal{K}_{m,n}$ with respect to \mathcal{K}_n , $\mathbf{r}_{m,n}$ denotes the position vector pointing from the origin of \mathcal{K}_n to that of $\mathcal{K}_{m,n}$.

Substituting Eq. (7), Eq. (10) and Eq. (12) into Eq. (8), leads to the stiffness model of the n th passive joint

$$\mathbf{f}_n = \mathbf{K}_n \boldsymbol{\zeta}_n = \mathbf{K}_n \begin{bmatrix} \mathbf{1}_6 & -\mathbf{1}_6 \end{bmatrix} \begin{pmatrix} \boldsymbol{\zeta}_{u,i} \\ \boldsymbol{\zeta}_{v,j} \end{pmatrix} \quad (14)$$

$$\mathbf{K}_n = \mathbf{W}_n \bar{\mathbf{K}}_n \mathbf{W}_n^T, \quad \bar{\mathbf{K}}_n = \left(\mathbf{W}_n^T \left(\sum_{m=1}^{M_n} \mathbf{T}_{m,n} \mathbf{K}_{m,n}^{-1} \mathbf{T}_{m,n}^T \right) \mathbf{W}_n \right)^{-1}$$

where $\mathbf{K}_n \in \mathbb{R}^{6 \times 6}$ denotes the Cartesian stiffness matrix of the n th passive joint, and $\bar{\mathbf{K}}_n \in \mathbb{R}^{(6-M_n) \times (6-M_n)}$ is referred to as the interface stiffness matrix that has the same structure to the stiffness matrix of a M_n DOF serial kinematic chain.

3.1.3 The reduced dynamic model of the parallel mechanism

Assembling super-element models of all substructures and the stiffness models of all passive joints by a lookup table that relates the local identifiers of interface nodes with the global identifiers of the passive joints involved, results in the partitioned dynamic model of the parallel mechanism.

$$\begin{bmatrix} \mathbf{M}_{\xi_p \xi_p} & \mathbf{M}_{\xi_p q} & \mathbf{M}_{\xi_p \eta} \\ & \mathbf{M}_{qq} & \mathbf{M}_{q\eta} \\ \text{sym} & & \mathbf{M}_{\eta\eta} \end{bmatrix} \begin{pmatrix} \ddot{\boldsymbol{\zeta}}_P \\ \ddot{\mathbf{q}} \\ \ddot{\boldsymbol{\eta}} \end{pmatrix} + \begin{bmatrix} \mathbf{K}_{\xi_p \xi_p} & \mathbf{K}_{\xi_p q} & \mathbf{K}_{\xi_p \eta} \\ & \mathbf{K}_{qq} & \mathbf{K}_{q\eta} \\ \text{sym} & & \mathbf{K}_{\eta\eta} \end{bmatrix} \begin{pmatrix} \boldsymbol{\zeta}_P \\ \mathbf{q} \\ \boldsymbol{\eta} \end{pmatrix} = \begin{pmatrix} \mathbf{f}_P \\ \mathbf{0} \\ \mathbf{0} \end{pmatrix} \quad (15)$$

$$\mathbf{q} = (\mathbf{q}_1^T \quad \mathbf{q}_2^T \quad \mathbf{q}_3^T)^T \in \mathbb{R}^6, \quad \mathbf{q}_i = (p_{1,i} \quad p_{2,i})^T \in \mathbb{R}^2, \quad i = 1, 2, 3$$

where $\mathbf{M}_{\xi_p \xi_p}$, $\mathbf{M}_{\xi_p q}$, $\mathbf{M}_{\xi_p \eta}$, \mathbf{M}_{qq} , $\mathbf{M}_{q\eta}$ and $\mathbf{M}_{\eta\eta}$ ($\mathbf{K}_{\xi_p \xi_p}$, $\mathbf{K}_{\xi_p q}$, $\mathbf{K}_{\xi_p \eta}$, \mathbf{K}_{qq} , $\mathbf{K}_{q\eta}$ and $\mathbf{K}_{\eta\eta}$) represent the partitioned mass (stiffness) matrices associated with the generalized coordinates $(\boldsymbol{\zeta}_P^T \quad \mathbf{q}^T \quad \boldsymbol{\eta}^T)^T$; $\mathbf{f}_P = \mathbf{f}_{2,4} \in \mathbb{R}^6$ and $\boldsymbol{\zeta}_P = \boldsymbol{\zeta}_{2,4} \in \mathbb{R}^6$ denote the interface nodal force and deflection vectors at P ($A_{2,4}$); $\mathbf{q} \in \mathbb{R}^6$ denotes the collection of all the internal modal coordinates corresponding to the first-order bending modes of three actuated limbs; $\boldsymbol{\eta}$ denotes the collection of the rest interface nodal deflection vectors and internal modal coordinates not belonging to either $\boldsymbol{\zeta}_P$ or \mathbf{q} .

In order to describe lower-order dynamic behaviors of the system using a minimum set of generalized coordinates, static condensation technique [34] is now applied to Eq. (15) by taking $\boldsymbol{\zeta}_P$ and \mathbf{q} as the master coordinates, and $\boldsymbol{\eta}$ as the slave coordinates. This treatment leads to the reduced dynamic model of the parallel mechanism while keeping its symbolic notions given in Eq. (15) unchanged for convenience.

$$\begin{bmatrix} \mathbf{M}_{\xi_p \xi_p} & \mathbf{M}_{\xi_p q} \\ \text{sym} & \mathbf{M}_{qq} \end{bmatrix} \begin{pmatrix} \ddot{\boldsymbol{\zeta}}_P \\ \ddot{\mathbf{q}} \end{pmatrix} + \begin{bmatrix} \mathbf{K}_{\xi_p \xi_p} & \mathbf{K}_{\xi_p q} \\ \text{sym} & \mathbf{K}_{qq} \end{bmatrix} \begin{pmatrix} \boldsymbol{\zeta}_P \\ \mathbf{q} \end{pmatrix} = \begin{pmatrix} \mathbf{f}_P \\ \mathbf{0} \end{pmatrix} \quad (16)$$

where

$$\begin{bmatrix} \mathbf{M}_{\xi_p \xi_p} & \mathbf{M}_{\xi_p q} \\ \text{sym} & \mathbf{M}_{qq} \end{bmatrix} = \begin{bmatrix} \mathbf{1}_6 & \mathbf{0} \\ \mathbf{0} & \mathbf{1}_6 \\ & \mathbf{B} \end{bmatrix}^T \begin{bmatrix} \mathbf{M}_{\xi_p \xi_p} & \mathbf{M}_{\xi_p q} & \mathbf{M}_{\xi_p \eta} \\ & \mathbf{M}_{qq} & \mathbf{M}_{q\eta} \\ \text{sym} & & \mathbf{M}_{\eta\eta} \end{bmatrix} \begin{bmatrix} \mathbf{1}_6 & \mathbf{0} \\ \mathbf{0} & \mathbf{1}_6 \\ & \mathbf{B} \end{bmatrix}$$

$$\begin{bmatrix} \mathbf{K}_{\xi_P \xi_P} & \mathbf{K}_{\xi_P q} \\ \text{sym} & \mathbf{K}_{qq} \end{bmatrix} = \begin{bmatrix} \mathbf{1}_6 & \mathbf{0} \\ \mathbf{0} & \mathbf{1}_6 \\ & \mathbf{B} \end{bmatrix}^T \begin{bmatrix} \mathbf{K}_{\xi_P \xi_P} & \mathbf{K}_{\xi_P q} & \mathbf{K}_{\xi_P \eta} \\ \text{sym} & \mathbf{K}_{qq} & \mathbf{K}_{q\eta} \\ & & \mathbf{K}_{\eta\eta} \end{bmatrix} \begin{bmatrix} \mathbf{1}_6 & \mathbf{0} \\ \mathbf{0} & \mathbf{1}_6 \\ & \mathbf{B} \end{bmatrix}, \quad \mathbf{B} = -\mathbf{K}_{\eta\eta}^{-1} \begin{bmatrix} \mathbf{K}_{\xi_P \eta} \\ \mathbf{K}_{q\eta} \end{bmatrix}^T$$

3.2 Dynamic Modeling of the Hybrid Robot

Equipped with the reduced dynamic model of the parallel mechanism developed in Section 3.1 at hand, this section formulates the dynamic model of the hybrid robot as a whole using screw theory and work-energy method.

As remarked in Ref. [27], the lower-order modes of the A/C wrist are primarily dominated by torsional compliances of its two actuated $\underline{\mathbf{R}}$ joints and inertias of its two rotary parts if the structural rigidities of these parts are assumed to be much higher than those of the actuated $\underline{\mathbf{R}}$ joints. The validity of this assumption has been verified by FE analysis addressed in [27]. Therefore, it is rational to model the wrist as a 2-DOF lumped mass-spring system shown in Fig.8 by taking account only of the torsional compliances of the transmission assemblies, with the other parts regarded as rigid bodies. Then, taking account of the deflection vector ξ_P of the platform at P , the addition theorem of instantaneous motions allows expressions of the absolute deflection vector $\xi_j \in \mathbb{R}^6$ of part j ($j=4$ for the C axis and $j=5$ for the A axis) at the same point, i.e.

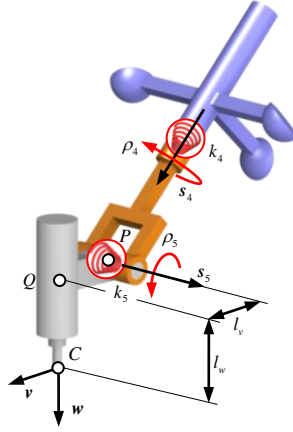


Fig.8. Lumped model of the A/C wrist

$$\xi_4 = \xi_P + \rho_4 \hat{\xi}_4 \quad (17)$$

$$\xi_5 = \xi_P + \rho_4 \hat{\xi}_4 + \rho_5 \hat{\xi}_5 \quad (18)$$

with

$$\hat{\xi}_4 = \begin{pmatrix} \mathbf{0} \\ s_4 \end{pmatrix}, \quad \hat{\xi}_5 = \begin{pmatrix} \mathbf{0} \\ s_5 \end{pmatrix}$$

where ρ_j and $\hat{\xi}_j \in \mathbb{R}^6$ ($j=4,5$) are the amplitude and unit twist of the j th axis with s_j being its unit vector. Accordingly, the following relationships hold

$$\begin{pmatrix} \xi_4 \\ \xi_5 \end{pmatrix} = \begin{bmatrix} \mathbf{1}_6 & \mathbf{0} & T_4 \\ \mathbf{1}_6 & \mathbf{0} & \mathbf{0} \end{bmatrix} \begin{pmatrix} \xi_5 \\ q \\ \rho \end{pmatrix}, \quad T_4 = \begin{bmatrix} \mathbf{0} & -\hat{\xi}_5 \end{bmatrix} \quad (19)$$

$$\begin{pmatrix} \xi_P \\ q \end{pmatrix} = \begin{bmatrix} \mathbf{1}_6 & \mathbf{0} & T_5 \\ \mathbf{0} & \mathbf{1}_6 & \mathbf{0} \end{bmatrix} \begin{pmatrix} \xi_5 \\ q \\ \rho \end{pmatrix}, \quad T_5 = \begin{bmatrix} -\hat{\xi}_4 & -\hat{\xi}_5 \end{bmatrix} \quad (20)$$

$$\rho = \begin{bmatrix} \mathbf{0} & \mathbf{0} & \mathbf{1}_2 \end{bmatrix} \begin{pmatrix} \xi_5 \\ q \\ \rho \end{pmatrix}, \quad \rho = \begin{pmatrix} \rho_4 \\ \rho_5 \end{pmatrix} \quad (21)$$

At this stage, replacing the work delivered by f_p on ξ_p using elastic potential and kinetic energies of the A/C wrist, allows elastic potential and kinetic energies of the hybrid robot as a whole to be expressed as

$$T = T_{\text{PM}} + T_{\text{WRIST}} = \frac{1}{2} \begin{pmatrix} \dot{\xi}_p \\ \dot{q} \end{pmatrix}^T \begin{bmatrix} \mathbf{M}_{\xi_p \xi_p} & \mathbf{M}_{\xi_p q} \\ \text{sym} & \mathbf{M}_{qq} \end{bmatrix} \begin{pmatrix} \dot{\xi}_p \\ \dot{q} \end{pmatrix} + \frac{1}{2} \begin{pmatrix} \dot{\xi}_4 \\ \dot{\xi}_5 \end{pmatrix}^T \begin{bmatrix} \mathbf{M}_4 & \\ & \mathbf{M}_5 \end{bmatrix} \begin{pmatrix} \dot{\xi}_4 \\ \dot{\xi}_5 \end{pmatrix} \quad (22)$$

$$V = V_{\text{PM}} + V_{\text{WRIST}} = \frac{1}{2} \begin{pmatrix} \xi_p \\ q \end{pmatrix}^T \begin{bmatrix} \mathbf{K}_{\xi_p \xi_p} & \mathbf{K}_{\xi_p q} \\ \text{sym} & \mathbf{K}_{qq} \end{bmatrix} \begin{pmatrix} \xi_p \\ q \end{pmatrix} + \frac{1}{2} \rho^T \mathbf{K}_\rho \rho, \quad \mathbf{K}_\rho = \begin{bmatrix} k_4 & \\ & k_5 \end{bmatrix} \quad (23)$$

where $\mathbf{M}_j \in \mathbb{R}^{6 \times 6}$ ($j=4,5$) denotes the mass matrix, evaluated at P in \mathcal{K} , of rotary part j , and k_j ($j=4,5$) denotes torsional stiffness coefficient of the transmission assembly of rotary part j , respectively.

In addition, let $\xi_C \in \mathbb{R}^6$ be the deflection vector evaluated in \mathcal{K}_C such that

$$\xi_5 = \mathbf{T}^{-1} \xi_C \quad (24)$$

with

$$\mathbf{T} = \begin{bmatrix} \mathbf{R} & r \times [\mathbf{R}] \\ \mathbf{0} & \mathbf{R} \end{bmatrix}, \quad r = -(l_v \mathbf{v} + l_w \mathbf{w})$$

where \mathbf{R} denotes the orientation matrix of \mathcal{K}_C with respect to \mathcal{K} , and $r = \overline{CP}$.

Finally, substituting Eqs. (19)-(21), (24) into Eqs. (22) and (23), and letting $f_C \in \mathbb{R}^6$ be the external wrench evaluated at C in \mathcal{K}_C , a cutting force for example, results in the dynamic model of the hybrid robot.

$$\mathbf{M} \ddot{\mathbf{x}} + \mathbf{K} \mathbf{x} = \mathbf{f} \quad (25)$$

$$\mathbf{M} = \begin{bmatrix} \mathbf{T}^{-T} \left(\sum_{j=4}^5 \mathbf{M}_j + \mathbf{M}_{\xi_p \xi_p} \right) \mathbf{T}^{-1} & \mathbf{T}^{-T} \mathbf{M}_{\xi_p q} & \mathbf{T}^{-T} \left(\mathbf{M}_{\xi_p \xi_p} \mathbf{T}_5 + \mathbf{M}_4 \mathbf{T}_4 \right) \\ & \mathbf{M}_{qq} & \mathbf{M}_{\xi_p q}^T \mathbf{T}_5 \\ \text{sym} & & \mathbf{T}_4^T \mathbf{M}_4 \mathbf{T}_4 + \mathbf{T}_5^T \mathbf{M}_{\xi_p \xi_p} \mathbf{T}_5 \end{bmatrix} \in \mathbb{R}^{14 \times 14}$$

$$\mathbf{K} = \begin{bmatrix} \mathbf{T}^{-T} \mathbf{K}_{\xi_p \xi_p} \mathbf{T}^{-1} & \mathbf{T}^{-T} \mathbf{K}_{\xi_p q} & \mathbf{T}^{-T} \mathbf{K}_{\xi_p \xi_p} \mathbf{T}_5 \\ & \mathbf{K}_{qq} & \mathbf{K}_{\xi_p q}^T \mathbf{T}_5 \\ \text{sym} & & \mathbf{K}_\rho + \mathbf{T}_5^T \mathbf{K}_{\xi_p \xi_p} \mathbf{T}_5 \end{bmatrix} \in \mathbb{R}^{14 \times 14}$$

$$\mathbf{x} = \begin{pmatrix} \xi_C^T & q^T & \rho^T \end{pmatrix}^T \in \mathbb{R}^{14}, \quad \mathbf{f} = \begin{pmatrix} f_C^T & \mathbf{0}^T & \mathbf{0}^T \end{pmatrix}^T \in \mathbb{R}^{14}$$

The dynamic model given in Eq. (25) is of fourteen generalized coordinates, including those for describing the first bend modes of three actuated limbs. This reduced model can be used to investigate the pose-varying dynamics of the hybrid robot in terms of modal analysis, contour error prediction, and cutting stability analysis of, for example, a milling process.

4. Verification

In this section, a full-size TriMule robot (see Fig.1) is taken as an exemplar to verify the effectiveness of the proposed approach. Equipped with parameters of the model developed in Eq. (25), the lower-order mode shapes and natural frequencies at the reference configuration (see Fig.9) are first evaluated and then compared with the results obtained by a full order FE model built by SAMCEF. Then, frequency response functions (FRFs) of the end-effector with/without considering the bending modes of three actuated limbs are investigated. Finally, natural frequencies across the reference plane of the task workspace are predicted with confidence.

Fig.9 shows the task workspace of the TriMule robot, which is defined as a cylinder of radius R and height h_1 plus a spherical crown of height h_2 that is internally tangent to the reachable envelope of point P . The reference

configuration is defined as that when $q_{3,1} = q_{3,2} = q_{3,3}$, $q_{3,4} = 0.5(q_{\min} + q_{\max})$ and $\theta_4 = \theta_5 = 0^\circ$. Here, q_{\max} and q_{\min} are the maximum and minimum lengths of the RP limb; θ_j ($j = 4, 5$) is the rotary angle of the j th actuated R joint of the wrist. The reference plane is defined as the cross section of the cylinder. The dimensional and workspace parameters of the robot are given in Table 1.

Table 1 Dimensional and workspace parameters of the TriMule robot.

a (m)	b_x (m)	b_y (m)	d (m)	H (m)	h_1 (m)	h_2 (m)	R (m)
0.135	0.320	0.570	0.190	1.000	0.240	0.220	0.600

Table 2 A lookup table and the compliance matrices of elastic elements in the passive joints.

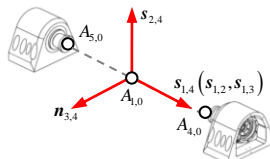
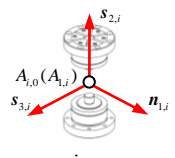
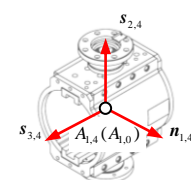
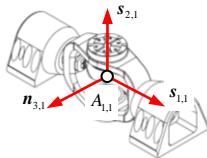
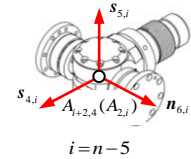
n	$K_{m,n}^{-1}$ (10^{-9} m/N or rad/(N·m))	W_n
 <p>R joint of support bearings ($n = 1$)</p>	$K_{1,1}^{-1} = \begin{bmatrix} 0.50 & -3.78 \times 10^{-4} & -4.35 \times 10^{-4} & -1.14 \times 10^{-3} & -4.21 \times 10^{-3} \\ & 2.51 & -9.09 \times 10^{-4} & 3.92 \times 10^{-3} & -8.76 \times 10^{-3} \\ & & 2.95 & 7.65 \times 10^{-3} & -1.17 \times 10^{-3} \\ & & & 1.95 & 2.77 \times 10^{-3} \\ \text{sym} & & & & 1.72 \end{bmatrix}$	$W_1 = \begin{bmatrix} s_{1,4} & s_{2,4} & n_{3,4} & \mathbf{0} & \mathbf{0} \\ \mathbf{0} & \mathbf{0} & \mathbf{0} & s_{2,4} & n_{3,4} \end{bmatrix}$ $n_{3,4} = s_{1,4} \times s_{2,4}$
 <p>R joint in <u>RPS</u> limbs ($n = 2, 3$)</p>	$K_{1,n}^{-1} = \begin{bmatrix} 1.22 & -1.11 \times 10^{-3} & 1.69 \times 10^{-2} & 7.93 \times 10^{-3} & 0.36 \\ & 1.76 & -4.32 \times 10^{-3} & -5.98 \times 10^{-2} & 1.23 \times 10^{-2} \\ & & 1.22 & 0.39 & -7.93 \times 10^{-3} \\ & & & 245.83 & -3.72 \\ \text{sym} & & & & 245.87 \end{bmatrix}$	$W_n = \begin{bmatrix} n_{1,i} & s_{2,i} & s_{3,i} & \mathbf{0} & \mathbf{0} \\ \mathbf{0} & \mathbf{0} & \mathbf{0} & n_{1,i} & s_{3,i} \end{bmatrix}$ $n_{1,i} = s_{2,i} \times s_{3,i}, \quad i = n$
 <p>RP joint in RP limb ($n = 4$)</p>	$K_{2,4}^{-1} = \begin{bmatrix} 7.69 & -1.44 \times 10^{-4} & -1.76 \times 10^{-3} & 5.07 \times 10^{-2} & 3.12 \times 10^{-2} \\ & 7.68 & 8.14 \times 10^{-4} & -9.73 \times 10^{-3} & 9.46 \times 10^{-3} \\ & & 344.82 & 5.07 \times 10^{-2} & -5.07 \times 10^{-2} \\ & & & 343.65 & 0.12 \\ \text{sym} & & & & 555.56 \end{bmatrix}$	$W_4 = \begin{bmatrix} n_{1,4} & s_{2,4} & \mathbf{0} & \mathbf{0} \\ \mathbf{0} & \mathbf{0} & s_{3,4} & n_{1,4} \end{bmatrix},$ $n_{1,4} = s_{2,4} \times s_{3,4}$
 <p>U joint in <u>UPS</u> limb ($n = 5$)</p>	$K_{1,5}^{-1} = \begin{bmatrix} 1.07 & -5.71 \times 10^{-5} & -1.47 \times 10^{-3} & -2.90 \times 10^{-3} & -0.26 \\ & 2.22 & -4.53 \times 10^{-3} & 1.12 \times 10^{-2} & -9.64 \times 10^{-2} \\ & & 1.25 & 7.07 \times 10^{-2} & -1.21 \times 10^{-2} \\ & & & 82.90 & 0.20 \\ \text{sym} & & & & 81.72 \end{bmatrix}$	$W_5 = \begin{bmatrix} s_{1,1} & s_{2,1} & n_{3,1} & \mathbf{0} \\ \mathbf{0} & \mathbf{0} & \mathbf{0} & n_{3,1} \end{bmatrix}$ $n_{3,1} = s_{1,1} \times s_{2,1}$
 <p>S joint in <u>RPS</u> and <u>UPS</u> limbs ($n = 6, 7, 8$)</p>	$K_{1,n}^{-1} = \begin{bmatrix} 1.85 & -1.58 \times 10^{-3} & -1.47 \times 10^{-3} & 7.93 \times 10^{-3} & -0.17 \\ & 1.85 & 1.69 \times 10^{-2} & 1.12 \times 10^{-2} & -6.64 \times 10^{-2} \\ & & 1.35 & 0.39 & -1.28 \times 10^{-2} \\ & & & 62.50 & 1.23 \times 10^{-2} \\ \text{sym} & & & & 62.50 \end{bmatrix}$ $K_{2,n}^{-1} = \begin{bmatrix} 6.48 & -1.5 \times 10^{-3} & 4.65 \times 10^{-3} & 1.23 \times 10^{-2} & -0.26 \\ & 10.08 & 4.08 \times 10^{-3} & -110.26 & -0.17 \\ & & 1.34 & 1.79 \times 10^{-2} & 4.10 \times 10^{-2} \\ & & & 4.62 \times 10^3 & 6.05 \\ \text{sym} & & & & 7.57 \times 10^3 \end{bmatrix}$	$W_n = \begin{bmatrix} s_{4,i} & s_{5,i} & n_{6,i} \\ \mathbf{0} & \mathbf{0} & \mathbf{0} \end{bmatrix}$ $n_{6,i} = s_{5,i} \times s_{4,i}, \quad i = n - 5$
$K_{3,n}^{-1} = \begin{bmatrix} 2.43 & -1.72 \times 10^{-3} & -1.79 \times 10^{-4} & -3.60 \times 10^{-2} & -4.75 \times 10^{-2} \\ & 5.66 & 2.35 \times 10^{-3} & -0.24 & 0.17 \\ & & 1.93 & -1.73 \times 10^{-2} & 0.18 \\ & & & 1.08 \times 10^3 & 1.21 \\ \text{sym} & & & & 2.54 \times 10^3 \end{bmatrix}$		

Table 3 Stiffness coefficients and inertial parameters of substructures in the parallel mechanism.

	<p>Inertial parameters (kg, m, kg · m²):</p> $m_0 = 115$ $\mathbf{I}_0 = \text{diag}[1.172 \quad 8.106 \quad 8.628]$
<p>Base link ($i = 0$)</p>	
	<p>Axial stiffness of \underline{P} joint (10^9 N/m):</p> $k_{\text{screw},i} = (k_{\text{nut}}^{-1} + k_{\text{rear}}^{-1} + k_{s,i}^{-1})^{-1}$ $k_{s,i} = EA / (q_{3,i} - l_1 + l_2), \quad k_{\text{nut}} = 0.30, \quad k_{\text{rear}} = 0.58$ $l_1 = 0.9 \text{ m}, \quad l_2 = 0.36 \text{ m}, \quad EA = 1.01 \times 10^8 \text{ N}$ <p>Cross section parameters (m):</p> $D_1 = 0.06, \quad d_1 = 0.04, \quad D_2 = 0.09, \quad d_2 = 0.076$
<p>Actuated limb ($i = 1, 2, 3$)</p>	
	<p>Inertial parameters of platform (kg, m, kg · m²):</p> $m_p = 64, \quad \mathbf{I}_p = \text{diag}[0.595 \quad 0.598 \quad 0.562]$ <p>Cross section parameters of central tube (m):</p> $D_3 = 0.131, \quad d_3 = 0.106, \quad l_3 = 1.24$ <p>Material properties:</p> <p>Density $\rho = 7800 \text{ kg/m}^3$, Elasticity $E = 210 \text{ Gpa}$</p> <p>Poisson ratio $\lambda = 0.28$</p>
<p>Passive limb ($i = 4$)</p>	

Table 4 Stiffness coefficients and inertial parameters of rotary parts in the wrist.

	<p>Inertial parameters (kg, m, kg · m²):</p> $m_4 = 32, \quad \mathbf{I}_4 = \begin{bmatrix} 0.403 & 0.07 & 0.053 \\ & 0.496 & 0.026 \\ \text{sym} & & 0.357 \end{bmatrix}$ <p>Torsional stiffness (10^6 N · m/rad): $k_4 = 0.337$</p>
<p>C-axis Rotary part of C-axis</p>	
	<p>Inertial parameters (kg, m, kg · m²):</p> $m_5 = 36.5, \quad \mathbf{I}_5 = \begin{bmatrix} 0.487 & 0.036 & 0.011 \\ & 0.434 & 0.023 \\ \text{sym} & & 0.192 \end{bmatrix}$ <p>Torsional stiffness (10^6 N · m/rad): $k_5 = 0.385$</p> $l_w = 0.22 \text{ m}, \quad l_v = 0.12 \text{ m}$
<p>A-axis Rotary part of A-axis</p>	

Table 2 shows a lookup table that links the passive joints with the interface nodes on substructures, and the relevant stiffness matrices of elastic elements in passive joints of the parallel mechanism. Tables 3 and 4 show relevant stiffness coefficients and inertial parameters of substructures of the parallel mechanism and rotary parts of the wrist, respectively. These data were obtained variously from design handbooks, product catalogs, and CAD/CAE software.

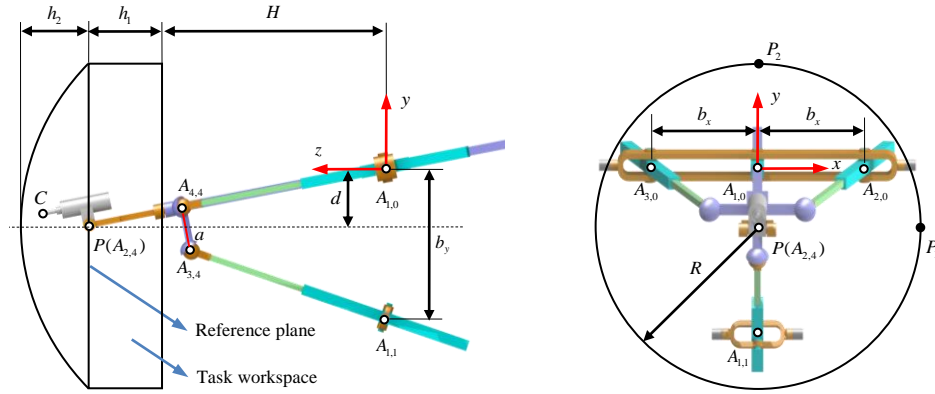


Fig.9. Task workspace of the TriMule robot

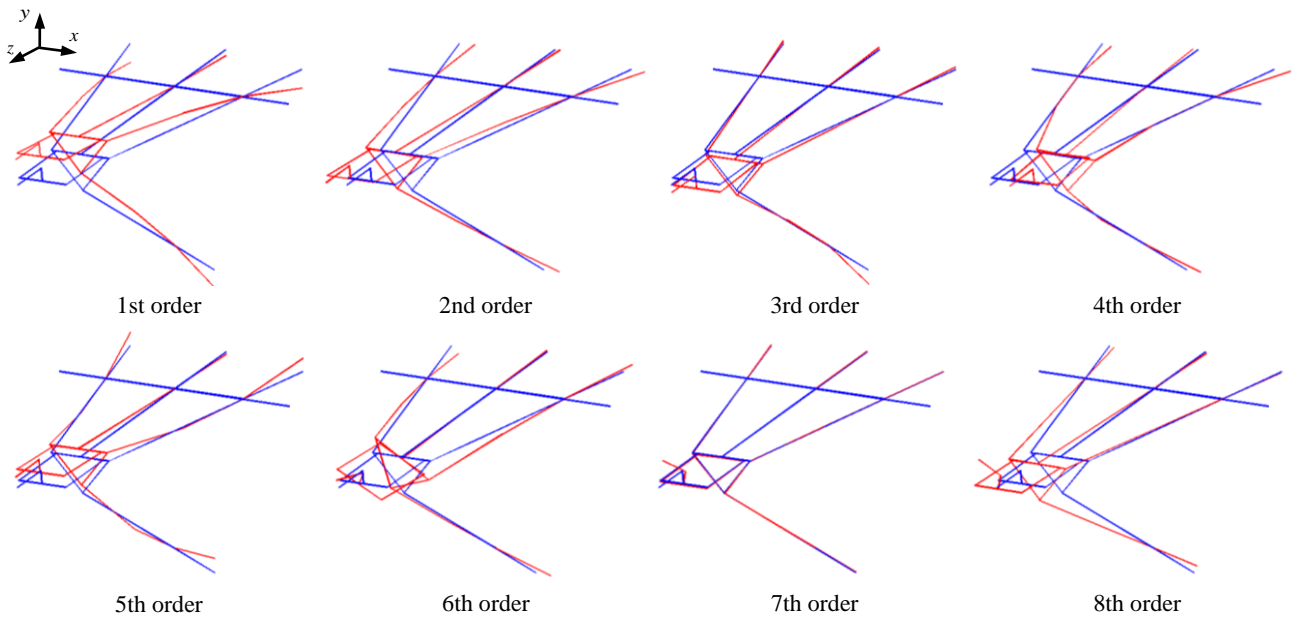


Fig.10. The first eighth lower-order mode shapes calculated by the proposed method

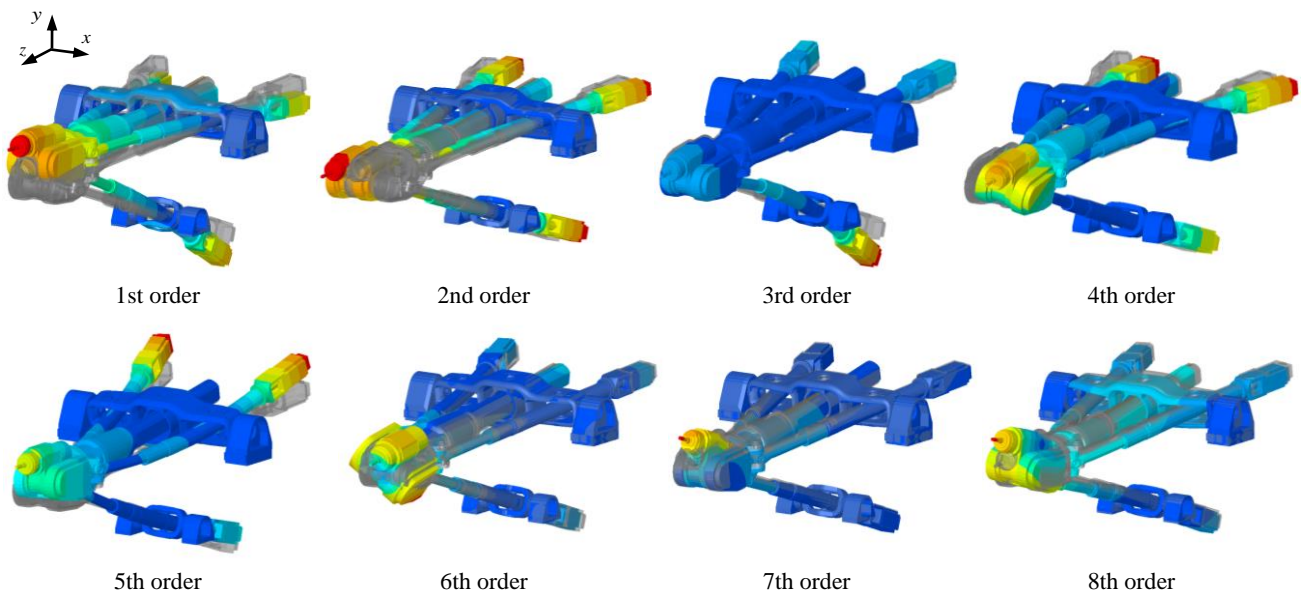


Fig.11. The first eighth lower-order mode shapes calculate by the FE model

Fig.10 shows the first eight mode shapes of the TriMule robot predicted by the proposed model at the reference configuration. Clearly, the 1st and 2nd modes are the bending vibrations caused by the axial deformation of the UPS limb as well as that of two RPS limbs. The 3rd-5th modes are the bending vibrations of three actuated limbs. The 6th mode is torsional vibrations of the RP limb and C-axis of the wrist, and the 7th mode is torsional vibration of the A-axis of the wrist. The 8th mode is translational vibration along the axial of the passive limb. To verify the computational accuracy of the proposed approach, an FE model is established by using commercial software SAMCEF. The corresponding stiffness and inertial parameters and boundary conditions in the model are set as consistent as possible to those used in the proposed model, leading to the FE model having 7.21×10^4 DOFs. Fig.11 shows the mode shapes predicted by the FE model, showing that results match well with those obtained by the proposed semi-analytical model.

Then, the Modal Assurance Criterion (MAC) [35] is employed to verify the consistency between mode shapes obtained by two models

$$\text{MAC}_{ij} = \frac{(\boldsymbol{\Phi}_{\text{FE},i}^T \boldsymbol{\Phi}_{\text{TH},j})^2}{(\boldsymbol{\Phi}_{\text{FE},i}^T \boldsymbol{\Phi}_{\text{FE},i})(\boldsymbol{\Phi}_{\text{TH},j}^T \boldsymbol{\Phi}_{\text{TH},j})} \quad (26)$$

where $\boldsymbol{\Phi}_{\text{FE},i}$ and $\boldsymbol{\Phi}_{\text{TH},j}$ are the i th and j th ($i, j = 1, 2, \dots, 8$) mode shapes calculated by the FE model and the proposed semi-analytical model, respectively. Fig.12 shows clearly that the values of diagonal elements are much larger than those of the non-diagonal elements (0.93 against 0.3), confirming the validity of the proposed model for predicting the lower-order dynamics of the robot.

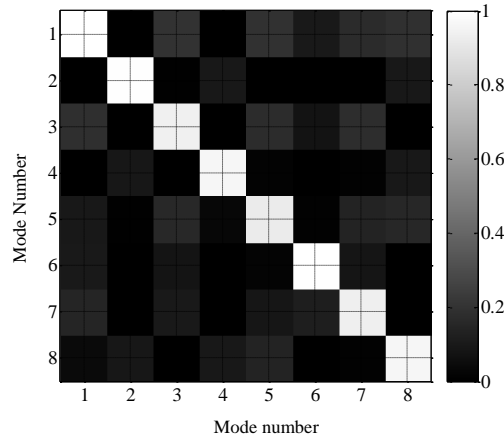


Fig.12. MAC of the first eighth mode shapes between the semi-analytical model and the FE model

Considering the pose dependent lower-order dynamic behaviors of hybrid robot, the natural frequencies at three typical configurations, i.e. $P(0 \ -d \ H+h_1)$, $P_1(R \ -d \ H+h_1)$ and $P_2(0 \ R-d \ H+h_1)$ are calculated by the method proposed here and the semi-analytical method proposed in Ref.[27]. Both will be examined by a full order FE model. It can be seen from Table 5 that the maximum discrepancies between the proposed model and FE model are less than 6% at the reference configuration and are less than 8% at the other two configurations. The computational accuracy of the proposed method is higher than that obtained by the method proposed in Ref. [27]. It is important to note that the 3rd-5th order modes caused by the local bending of three actuated limbs cannot be captured by the method proposed in Ref. [27].

Having been convinced by the effectiveness of the proposed model, the influence of bending modes of three actuated limbs on frequency response functions (FRFs) of the end-effector is investigated. Fig.13 shows FRFs of the tool center point (TCP) along the u , v and w axes of \mathcal{K}_C . They are obtained by the FE model, and proposed semi-analytical models with and without considering the bending modes (i.e., the 3rd-5th modes) of the actuated limbs (model 1 and model 2 as shown in Fig.13). The damping ratio for all modes is set to be 0.03 identically in three different models. Clearly, the FRFs calculated by the model considering the bending modes match very well with those calculated by the FE model, confirming the necessity to take into account these bending modes for precisely reflecting the lower-order dynamics of the robot.

Table 5 Natural frequencies calculated by the semi-analytical models and a full order FE model at different configurations.

Configuration\Mode order		1st	2nd	3rd	4th	5th	6th	7th	8th
P	FE	32.51	33.12	46.48	50.08	55.13	80.99	95.45	131.63
	SA 1	33.74	34.16	47.53	51.42	57.34	85.22	99.10	139.03
	ε_1	3.78	3.14	2.26	2.68	4.01	5.22	3.82	5.62
	SA 2	34.28	35.13	-	-	-	86.02	99.31	142.54
	ε_2	5.44	6.07	-	-	-	6.21	4.04	8.29
	FE	25.93	29.71	44.66	48.12	54.03	79.09	91.30	127.63
P_1	SA 1	26.97	30.88	45.89	49.52	56.35	84.32	96.62	137.46
	ε_1	4.01	3.94	2.75	2.91	4.29	6.61	5.83	7.70
	SA 2	27.61	31.67	-	-	-	85.97	96.70	140.49
	ε_2	6.48	6.60	-	-	-	8.70	5.91	10.08
	FE	25.21	31.27	43.64	48.96	54.99	78.44	92.05	128.22
	SA 1	26.29	32.55	44.96	50.47	57.13	83.98	97.22	137.68
P_2	ε_1	4.28	4.09	3.02	3.08	3.89	7.06	5.62	7.38
	SA 2	26.97	33.40	-	-	-	84.60	97.49	141.51
	ε_2	6.98	6.81	-	-	-	7.85	5.91	10.36

SA 1: semi-analytical model proposed in this paper; SA 2: semi-analytical model proposed in Ref.[27]. (Unit: Hz)

ε_1 (ε_2): discrepancy between SA 1(2) and a full FE model. (Unit: %)

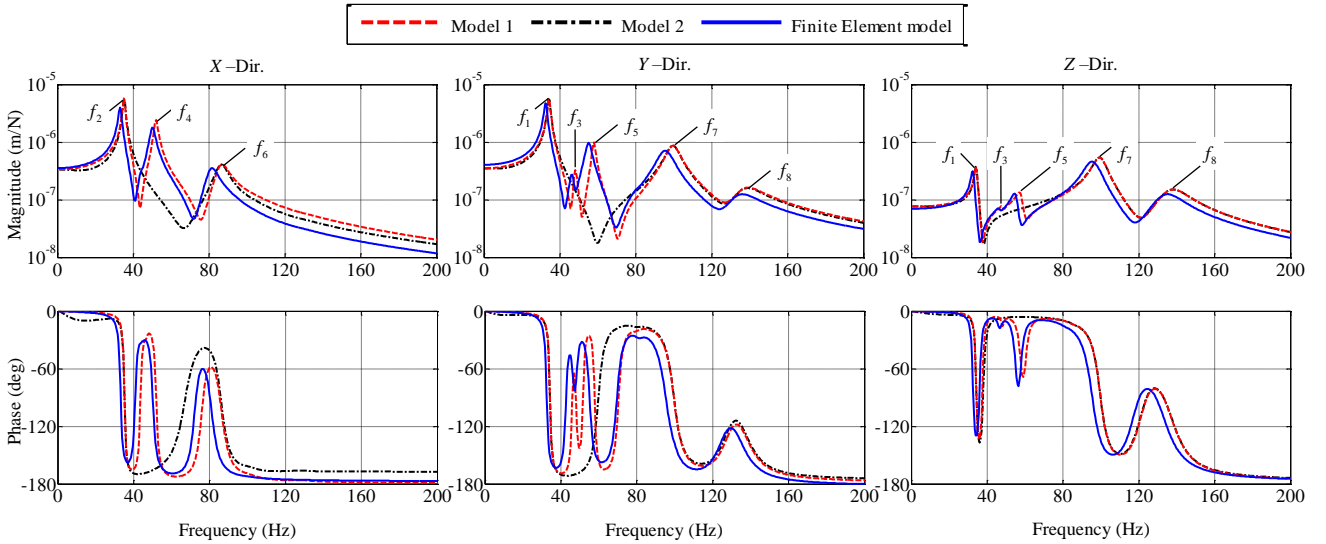


Fig.13. FRFs of two semi-analytical models and a full FE model

With the convincing results obtained at the reference configuration, dynamic behavior of the robot over the entire task workspace can be predicted. Fig.14 shows highly pose-varying natural frequency distributions across the reference plane, when keeping the spindle axis normal to the plane and the A-axis parallel to the x -axis. Clearly, all of them take the maximal values near the center of the plane and decrease monotonically down to the edge of the boundary.

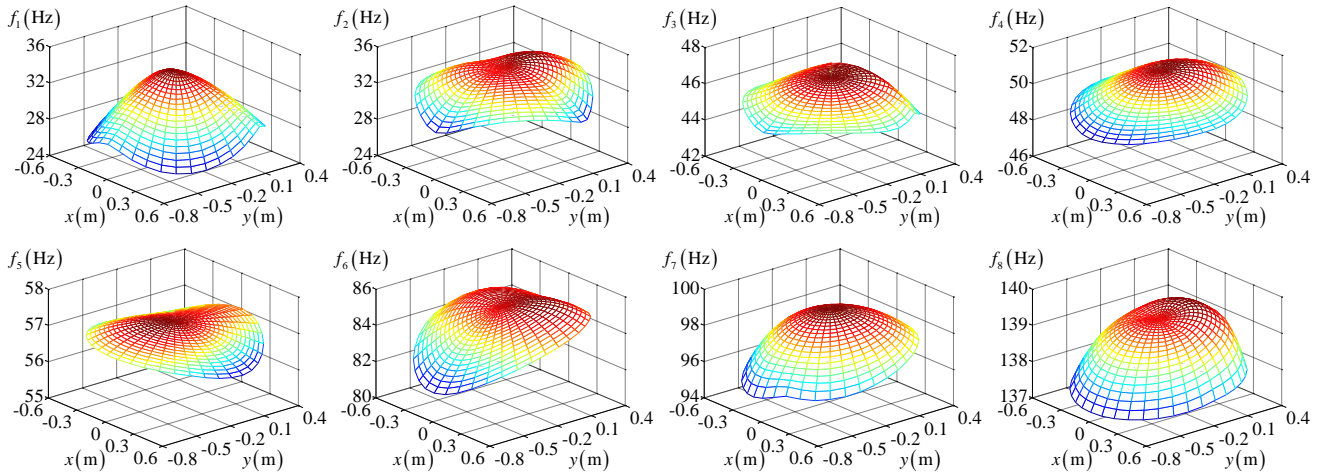


Fig.14. Natural frequencies distributions across the reference plane of the workspace

In order to demonstrate the computational efficiency of the proposed method, a comparison study is carried out on a workstation (Intel i5-3320M CPU and 8G RAM). It shows that the overall computational time used for solving eigenvalue problems at 720 poses is less than 18 seconds by using the proposed model compared with 43 seconds by using unreduced semi-analytical model. And 125 seconds is needed at a single configuration by using the FE model. As for FRFs analysis at a specific configuration, the overall computational time is less than 3.8 seconds for the proposed model compared with 13 seconds and 20 minutes for the unreduced semi-analytical model and FE model. These observations fully consolidate the usefulness of the proposed model for predicting pose-varying dynamic behavior, and thus for subsequently sensitivity analysis of dimensional and structural parameters as well as cutting stability analyses.

Finally, the SIMO (single input and multiple output) experimental modal test is carried out at reference configuration of a prototype machine to verify the proposed semi-analytical method. Fig.15 (a) shows the experimental setup where a LMS dynamic analyzer is used to process the force and vibration signals measured by impact hammer (B&K 8207) and accelerometer (PCB 356A26). Fig. 15(b) shows the locations of the excitation and pick-up points where the signals measured in the body-fixed local frames are transformed to the global frame so that the embedded curve fitting algorithm provided by the dynamic analyzer can be implemented to generate the appropriate FRFs and mode shapes.

In comparison of Fig. 13 with Fig. 16, it is easy to see the main features of the FRFs and mode shapes obtained by the experiment modal analysis can be fully captured by the semi-analytical method proposed though the natural frequencies of the realistic machine are lower than those obtained by the semi-analytical method.

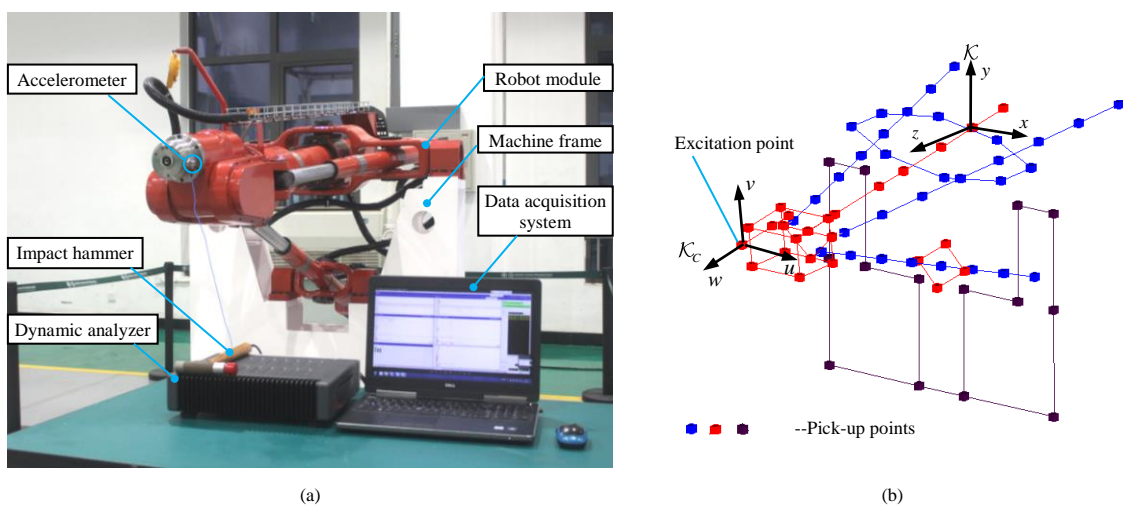


Fig.15. Experimental setup for FRF test: (a) Experimental setup, (b) Excitation and pick-up points

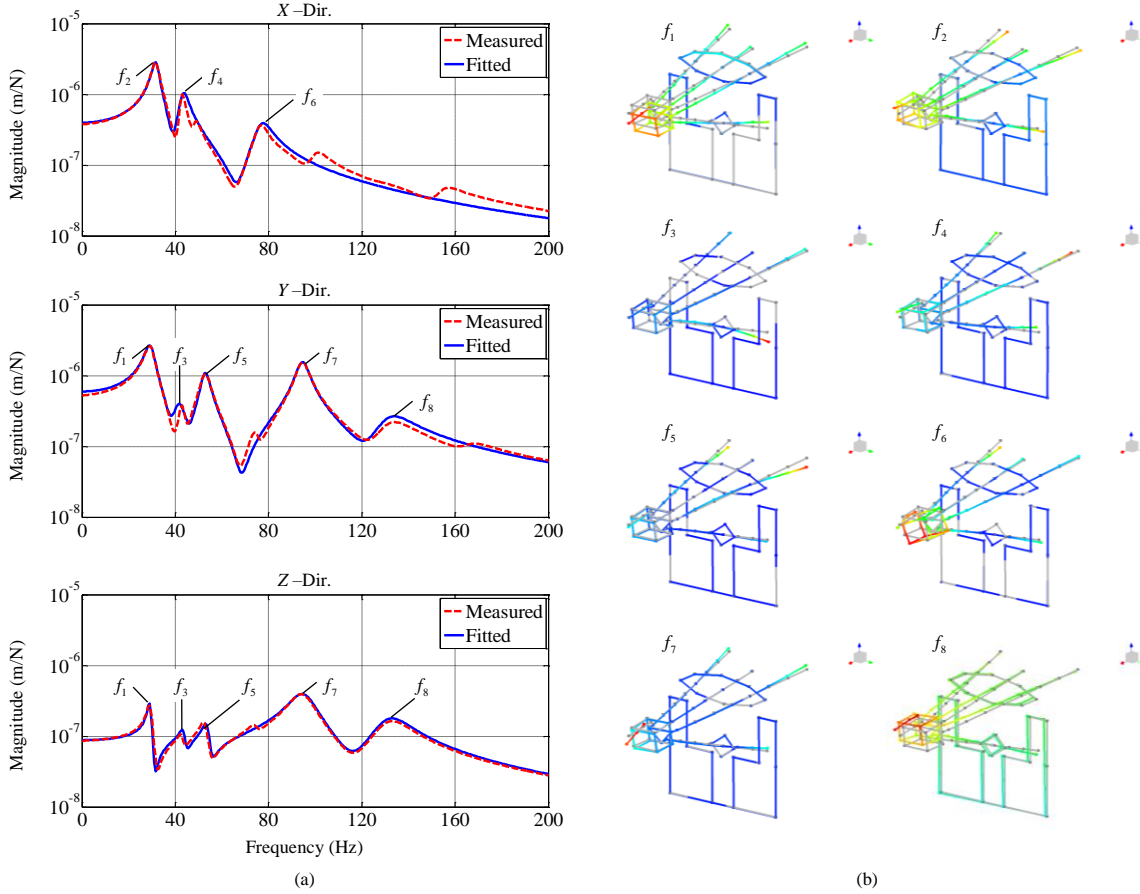


Fig.16. Experimental results of the TriMule hybrid robot: (a) FRFs at the end-effector, (b) Mode shapes

5. Conclusions

This paper presents an effective approach to predict the lower-order dynamics of a 5-DOF hybrid robot named TriMule that comprises a 3-DOF parallel mechanism and 2-DOF wrist. The conclusions are drawn as follows

(1) A semi-analytical approach has been presented for dynamic modeling of hybrid robots. By combining FEA with modal reduction technique, super-element models of both actuated and passive limb substructures within the parallel mechanism are first formulated. Then, a general stiffness model of multiple DOF passive joints connecting the substructures is derived using reciprocal/dual properties of twist/wrench system imposed upon these joints. These treatments lead to a reduced dynamic model of the parallel mechanism. Finally, merging the elastic potential and kinetic energies of the parallel mechanism and wrist, results in a dynamic model of the hybrid robot having fourteen generalized coordinates, including those for describing the first bending modes of three actuated limbs. These minimum set of generalized coordinates enable the full set of lower-order modes of hybrid robot to be predicted with sufficient accuracy and efficiency. Meanwhile, the method of stiffness modeling of multiple DOF passive joints proposed here is so general that it would potentially be useful for the dynamic modeling of other types of hybrid robots.

(2) By taking a full-size 5-DOF TriMule robot as an exemplar, the effectiveness of the proposed approach has been demonstrated by a comparison study against FEA software and experimental modal analysis. The results of eigenvalue and frequency response function analyses show that the full set of lower-order dynamics can be predicted with sufficient computational accuracy and huge computational time savings (over FEA) across the entire workspace. The proposed approach is thereby very useful in optimal design, contour error prediction as well as in cutting stability analysis of this brand new hybrid robot under the framework of digital twin technology.

Acknowledgement

This work is partially supported by National Key R&D program of China (Grant No. 2017YFB1301800), National Natural Science Foundation of China (grants 51622508 and 51420105007) and EU H2020-RISE-ECSASDP (grant 734272).

References

- [1] J. Thusty, J. Ziegert, S. Ridgeway, Fundamental comparison of the use of serial and parallel kinematics for machines tools, *CIRP Ann. - Manuf. Technol.* 48 (1999) 351–356.
- [2] M. Weck, D. Staimer, Parallel kinematic machine tools - Current state and future potentials, *CIRP Ann. - Manuf. Technol.* 51 (2002) 671–683.
- [3] L. Uriarte, M. Zatarain, D. Axinte, J. Yagüe-Fabra, S. Ihlenfeldt, J. Eguía, A. Olarra, Machine tools for large parts, *CIRP Ann. - Manuf. Technol.* 62 (2013) 731–750.
- [4] Y. Altintas, C. Brecher, M. Week, S. Witt, Virtual Machine Tool, *CIRP Ann. - Manuf. Technol.* (2005).
- [5] H. Son, H.J. Choi, H.W. Park, Design and dynamic analysis of an arch-type desktop reconfigurable machine, *Int. J. Mach. Tools Manuf.* 50 (2010) 575–584.
- [6] D. Zhang, Z. Gao, Performance analysis and optimization of a five-degrees-of-freedom compliant hybrid parallel micromanipulator, *Robot. Comput. Integr. Manuf.* 34 (2015) 20–29.
- [7] Y. Ma, W. Niu, Z. Luo, F. Yin, T. Huang, Static and dynamic performance evaluation of a 3-DOF spindle head using CAD–CAE integration methodology, *Robot. Comput. Integr. Manuf.* 41 (2016) 1–12.
- [8] D. Hong, S. Kim, W.C. Choi, J.B. Song, Analysis of machining stability for a parallel machine tool, *Mech. Based Des. Struct. Mach.* 31 (2003) 509–528.
- [9] I. Tyapin, G. Hovland, The Gantry-Tau parallel kinematic machine-kinematic and elastodynamic design optimisation, *Meccanica.* 46 (2011) 113–129.
- [10] J. Wu, X. Chen, T. Li, L. Wang, Optimal design of a 2-DOF parallel manipulator with actuation redundancy considering kinematics and natural frequency, *Robot. Comput. Integr. Manuf.* 29 (2013) 80–85.
- [11] V.T. Portman, V.S. Chapsky, Y. Shneur, Evaluation and optimization of dynamic stiffness values of the PKMs: Collinear stiffness value approach, *Mech. Mach. Theory.* 74 (2014) 216–244.
- [12] G. Piras, W.L. Cleghorn, J.K. Mills, Dynamic finite-element analysis of a planar high-speed, high-precision parallel manipulator with flexible links, *Mech. Mach. Theory.* 40 (2005) 849–862.
- [13] Y. Zhao, F. Gao, X. Dong, X. Zhao, Dynamics analysis and characteristics of the 8-PSS flexible redundant parallel manipulator, *Robot. Comput. Integr. Manuf.* 27 (2011) 918–928.
- [14] A. Cammarata, D. Condorelli, R. Sinatra, An Algorithm to Study the Elastodynamics of Parallel Kinematic Machines With Lower Kinematic Pairs, *J. Mech. Robot.* 5 (2012) 011004.
- [15] A. Cammarata, I. Caliò, D. D'Urso, A. Greco, M. Lacagnina, G. Fichera, Dynamic stiffness model of spherical parallel robots, *J. Sound Vib.* 384 (2016) 312–324.
- [16] B. Lian, L. Wang, X.V. Wang, Elastodynamic modeling and parameter sensitivity analysis of a parallel manipulator with articulated traveling plate, *Int. J. Adv. Manuf. Technol.* (2019).
- [17] C.M. Gosselin, D. Zhang, Stiffness analysis of parallel mechanisms using a lumped model, *Int. J. Rob. Res.* 17 (1998) 17–27.
- [18] S. Briot, A. Pashkevich, D. Chablat, On the optimal design of parallel robots taking into account their deformations and natural frequencies, *Proc. ASME Des. Eng. Tech. Conf.* 7 (2009) 367–376.
- [19] S.-K. Zhu, Y.-Q. Yu, Pseudo-Rigid-Body Model for the Flexural Beam With an Inflection Point in Compliant Mechanisms, *J. Mech. Robot.* 9 (2017) 031005.
- [20] P. Bilancia, G. Berselli, L. Bruzzone, P. Fanghella, A CAD/CAE integration framework for analyzing and designing spatial compliant mechanisms via pseudo-rigid-body methods, *Robot. Comput. Integr. Manuf.* 56 (2019) 287–302.
- [21] X. Wang, J.K. Mills, Dynamic modeling of a flexible-link planar parallel platform using a substructuring approach, *Mech. Mach. Theory.* 41 (2006) 671–687.
- [22] M. Law, S. Ihlenfeldt, M. Wabner, Y. Altintas, R. Neugebauer, Position-dependent dynamics and stability of serial-parallel kinematic machines, *CIRP Ann. - Manuf. Technol.* 62 (2013) 375–378.
- [23] D. Liang, Y. Song, T. Sun, X. Jin, Rigid-flexible coupling dynamic modeling and investigation of a redundantly actuated parallel manipulator with multiple actuation modes, *J. Sound Vib.* 403 (2017) 129–151.
- [24] L. Wu, G. Wang, H. Liu, T. Huang, An approach for elastodynamic modeling of hybrid robots based on substructure synthesis technique, *Mech. Mach. Theory.* 123 (2018) 124–136.
- [25] S. Briot, A. Pashkevich, D. Chablat, Reduced elastodynamic modelling of parallel robots for the computation of their natural frequencies, 13th World Congress in Mechanism & Machine Science (2011) 1–8.
- [26] J. Zhang, J.S. Dai, T. Huang, Characteristic Equation-Based Dynamic Analysis of a Three-Revolute Prismatic Spherical Parallel Kinematic Machine, *J. Comput. Nonlinear Dyn.* 10 (2014) 021017.
- [27] C. Dong, H. Liu, T. Huang, D.G. Chetwynd, A Screw Theory-Based Semi-Analytical Approach for Elastodynamics of the Tricept Robot, *J. Mech. Robot.* 11 (2019) 031005.
- [28] E. Wittbrodt, I. Adamić-Wójci, S. Wojciech, Dynamics of Flexible Multibody Systems, Springer Berlin Heidelberg, 2006.
- [29] T. Huang, C. Dong, H. Liu, X. Qin, J. Mei, Q. Liu, M. Wang, Five-degree-of-freedom parallel robot with multi-shaft rotary brackets, *Pub. No. WO/2017/005015 A1*, 2017.
- [30] T. Huang, C. Dong, H. Liu, T. Sun, D.G. Chetwynd, A simple and visually orientated approach for type synthesis of overconstrained 1T2R parallel mechanisms, *Robotica.* (2018) 1–13.
- [31] C. Farhat, M. Geradin, On a component mode synthesis method and its application to incompatible substructures, *Comput. Struct.* 51 (1994) 459–473.
- [32] M.I. Friswell, S.D. Garvey, J.E.T. Penny, Model reduction using dynamic and iterated IRS techniques, *J. Sound Vib.* 186 (1995) 311–323.
- [33] G. Masson, B. Ait Brik, S. Cogan, N. Bouhaddi, Component mode synthesis (CMS) based on an enriched ritz approach for efficient structural optimization, *J. Sound Vib.* 296 (2006) 845–860.
- [34] R.J. Guyan, Reduction of stiffness and mass matrices, *AIAA J.* 3 (1965) 380.
- [35] D. J. Ewins, Modal testing: theory, practice, and application, Research Sstudies Press, Baldok, Hertfordshire, UK, 2000.